A CASE STUDY FOR STACK-BASED CONTROL SOLUTIONS IN MOBILE INVERTED PENDULUM ROBOTS: DESIGN AND PERFORMANCE INSIGHTS

Dorin-Mihail DINULESCU[1]

[1]*Polytechnic University of Milan, e-mail: dorinmihail.dinulescu@mail.polimi.it*

Abstract: *This study examines the mechanical rationale behind the adoption of stack-based designs for mobile inverted pendulum robots. The stack configuration enhances stability by centering mass along the vertical axis, optimizing the robot's moment of inertia, and ensuring uniform weight distribution. It also minimizes spatial footprint, simplifies structural design, and provides flexibility for modular extensions. By prioritizing compactness and mechanical efficiency, the stack design supports critical stability requirements while accommodating additional components without compromising performance. This work highlights the functional and practical advantages of the stack solution, offering insights for future developments in mobile robot design.*

Keywords: *Mobile inverted pendulum robots, Stack-based design, Mechanical stability, Modular robot architecture, Compact robot structures.*

1. Introduction

An inverted pendulum robot is a type of self-balancing system that operates on the principle of maintaining an unstable equilibrium by constantly adjusting its position through precise control algorithms and actuators. These types of mechatronic systems have garnered significant attention in robotics due to their unique dynamic balancing capabilities and wide range of applications, from transportation to research and education. Designing such robots involves overcoming critical challenges, particularly in achieving mechanical stability and efficient weight distribution.

This paper presents an analysis of the structural mechanics and center of mass positioning for a custom-designed mobile inverted pendulum robot. Through detailed resistance calculations and mass distribution studies, the research explores how a stack-based configuration optimizes stability and functionality. The findings demonstrate the practical advantages of this design approach, providing valuable insights for future improvements.

2. Mass centering and stability

The success of an inverted pendulum robot hinges on its ability to maintain dynamic balance. By aligning the mass as close as possible to the vertical axis of rotation, the stack design minimizes destabilizing forces that arise during movement or external disturbances. The key benefits are:

1. reduced torque requirements: a centered mass requires less corrective torque from the actuators to counterbalance the pendulum's tilt, allowing for smaller and more efficient motors.
2. improved response time: the closer the center of mass is to the rotation axis, the lower the inertia, enabling faster adjustments to maintain stability during sudden accelerations, decelerations, or external impacts.
3. enhanced durability: a stable and well-balanced design reduces wear and tear

on structural and motor components, prolonging the robot's operational life.

For the mobile inverted pendulum robot, the center of gravity value is essential for determining the motor characteristics needed to balance the mass. Moreover, positioning the center of gravity as close as possible to the motor axis favors balance, significantly reducing energy consumption and enabling faster motor response. A lower center of gravity is directly proportional to the system's stability. The kinematic diagram of the system can be described as follows:

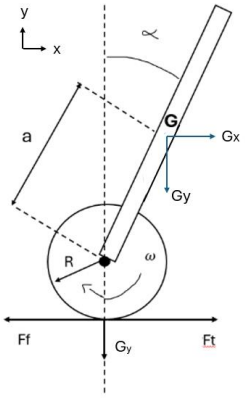

Figure 1: *Kinematic diagram of the mechatronic system (Ft – traction force; Ff – friction force; R – wheel radius; a – distance from the center of gravity to the motor axis; α – maximum tilt angle, chosen at 30 degrees; G – center of gravity of the system (with Vertical component of the weight and horizontal component of the weight; ω–angular velocity).*

After performing the corresponding calculations and measurements, the resulting value is G = 9.633 N, where m = 0.982 kg and g = 9.81 m/s².

For maximum accuracy in calculating the center of gravity, the design environment SolidWorks was used, which includes an option to simulate the positioning of the system's center of gravity, regardless of the assembly's complexity. The design included all the elements necessary for the system's operation. These were scaled to real dimensions and weighed to ensure the robot's sizing was as accurate as possible. Both structural assemblies and significantly massive electronic components, such as the battery, were included. The value of interest is the center of gravity's coordinate relative to the motor axis along the Oy axis, which is +33.47 mm.

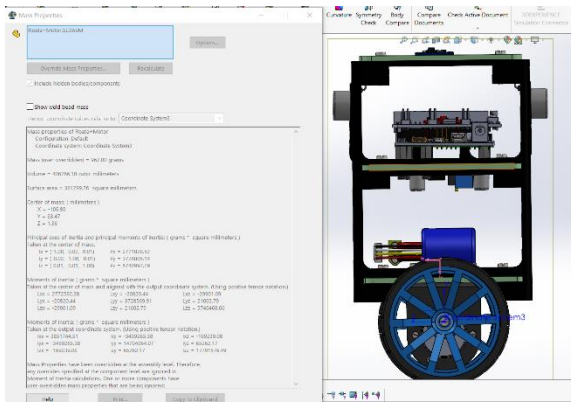

Figure 2: *Position of the center of gravity and system mass*

3. Uniform distribution of loads

In the process of designing and building a mobile robot with an inverted pendulum structure configured in a three-level stack, a critical aspect to consider is the calculation of the structural strength. This is essential to ensure the robot functions correctly and safely under various operating conditions.

The structural strength calculation is necessary to determine the ability of the structure to withstand the mechanical loads and stresses it will encounter during use. Because the inverted pendulum mobile robot will be subjected to varying movements and accelerations, the structure must be robust enough to resist these conditions.

Under these considerations, the strength of the robot’s casing is calculated. Factors such as the material used, geometry, load distribution, and safety factors involved in the design are taken into account. By performing this strength calculation, the structure's capacity to handle specific mechanical loads and stresses can be evaluated and validated, ensuring optimal and safe performance in diverse usage scenarios.

Thus, in the XOY plane, a symmetrical mechanical structure is considered, with different weights distributed on each plate embedded in two bars at each end of these plates.

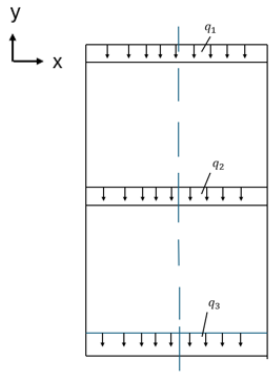

Figure 3: *Equivalence of the robot's structural resistance.*

To simplify the problem, the calculation scheme can be reduced by sectioning the entire structure at its midpoint, applying a moment (M), shear forces (T), and an axial force (N) on each bar, except for the first one, which is considered embedded to support the structure.

Since the structure is geometrically and load-symmetrical, the axial and moment diagrams are symmetrical, and the shear force diagram is antisymmetric, resulting in zero shear force along the axis of symmetry.

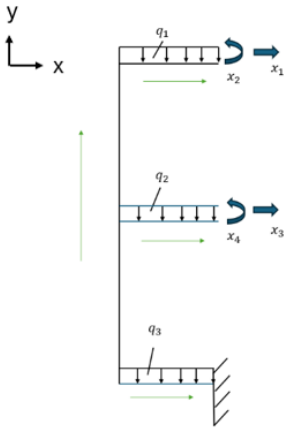

Figure 4: *Base system of the structural resistance schematization of the robot.*

L becomes l/2 as a result of sectioning the plate along its midpoint ($g=9.81\ m/s^2$ where g represents gravitational acceleration).

It follows that:

$$F = m \cdot g \tag{1}$$

$$q = \frac{F}{2 \cdot L} \tag{2}$$

Where q represents the uniformly distributed force equivalent to the load on the structure.

$$m_1 = 165\ g => F = 1.62\ N \tag{3}$$

$$m_2 = 80\ g => F = 0.78\ N \tag{4}$$

$$m_3 = 50\ g => F = 0.49\ N \tag{5}$$

L = 70 mm = 0.07 m.

$h_1 = h_2 = 50$ mm = 0.05 m.

$$q_1 = \frac{1.62\ N}{2 \cdot 70\ mm} = 11.57\ \frac{N}{m} \tag{6}$$

$$q_2 = \frac{0.78\ N}{2 \cdot 70\ mm} = 5.57\ \frac{N}{m} \tag{7}$$

$$q_3 = \frac{0.49\ N}{2 \cdot 70\ mm} = 3.5\ \frac{N}{m} \tag{8}$$

$$x_1 = x_2 = x_3 = x_4 = 0 \tag{9}$$

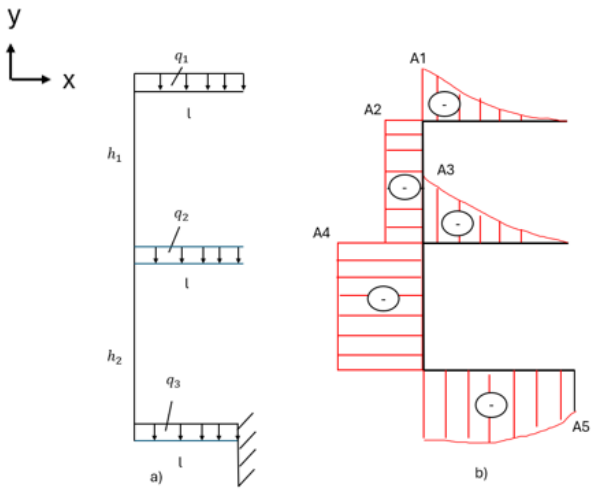

Figure 5: *a) System 0 and b) the moment diagram of System 0.*

Values for points A_1, A_2, A_3, A_4, A_5:

$$A_1 = \frac{q_1 \cdot l^2}{2} \tag{10}$$

$$A_2 = \frac{q_1 \cdot l^2}{2} + \frac{q_2 \cdot l^2}{2} \tag{11}$$

$$A_3 = \frac{q_2 \cdot l^2}{2} \tag{12}$$

$$A_4 = \left(q_2 \cdot \frac{l^2}{2} + q_1 \cdot \frac{l^2}{2}\right) \tag{13}$$

$$A_5 = \left(q_2 \cdot \frac{l^2}{2} + q_1 \cdot \frac{l^2}{2}\right) + q_3 \cdot \frac{l^2}{2} \tag{14}$$

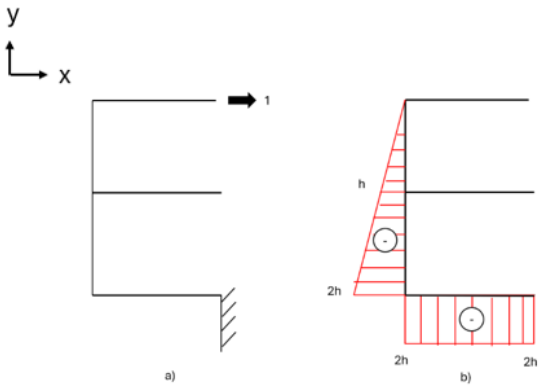

Figure 6: *a) System x_1 and b) the moment diagram of system $x_1 = 1$.*

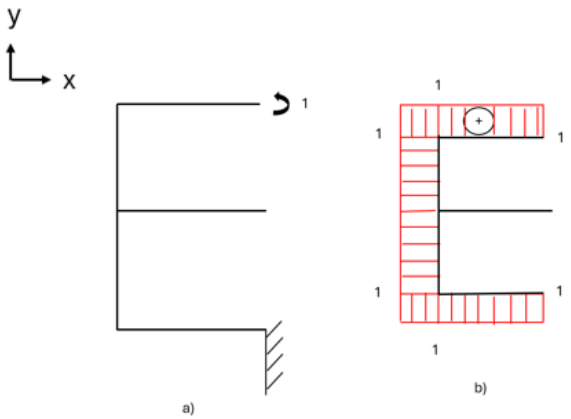

Figure 7: *a) System x_2 and b) the moment diagram of system $x_2 = 1$.*

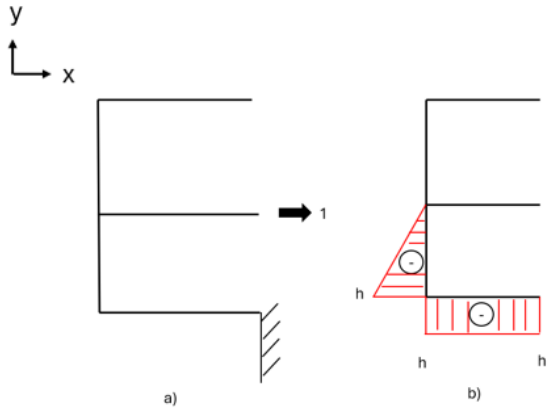

Figure 8: *a) System x_3 and b) the moment diagram of system $x_3 = 1$.*

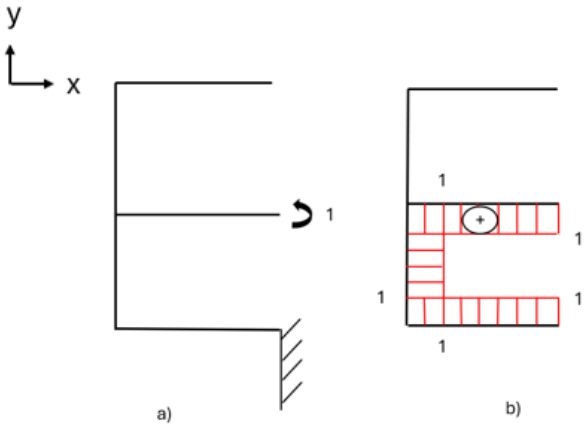

Figure 9: *a) System x_4 and b) the moment diagram of system $x_4 = 1$.*

Matrix for the calculation of displacements:

$$\delta_{10} + x_1\delta_{11} + x_2\delta_{12} + x_3\delta_{13} + x_4\delta_{14} = 0 \tag{15}$$

$$\delta_{20} + x_1\delta_{21} + x_2\delta_{22} + x_3\delta_{23} + x_4\delta_{24} = 0 \tag{16}$$

$$\delta_{30} + x_1\delta_{31} + x_2\delta_{32} + x_3\delta_{33} + x_4\delta_{34} = 0 \tag{17}$$

$$\delta_{40} + x_1\delta_{41} + x_2\delta_{42} + x_3\delta_{43} + x_4\delta_{44} = 0 \tag{18}$$

$$\delta_{10} + x_1\delta_{11} + x_2\delta_{12} + x_3\delta_{13} + x_4\delta_{14} = 0 \tag{19}$$

Where: $\delta_{ij} = \delta_{ji}$.

$$EI_y\delta = \frac{l_i}{6}\left[\left(M_S + M_D \pm \frac{p * l_i^2}{4}\right) * (m_S + m_D) + M_S m_S + M_D m_D\right] \quad (20)$$

Where:

1. EI_y represents the bending rigidity.
2. l_i is the length of interval iii.
3. M_S is the moment on the left side of the interval from the MMM diagram.
4. M_D is the moment on the right side of the interval from the MMM diagram.
5. m_S is the moment on the left side of the interval from the mmm diagram.
6. m_D is the moment on the right side of the interval from the mmm diagram.
7. p is the intensity of the distributed force along the respective interval.

After substituting the above-mentioned values into the equations and performing the corresponding calculations, the following results are obtained: δ_{10} = 0.526 Nmm^2; δ_{11} = 0.001033333 mm^3; $\delta_{12} = \delta_{21}$ = -0.012 mm^2; $\delta_{13} = \delta_{31}$ = 0.000454167 mm^3; $\delta_{14} = \delta_{41}$ = 0.01075 mm^2; $\delta_{24} = \delta_{42}$ = 0.12 mm; δ_{30} = 0.000219508 Nmm^3; δ_{33} = 0.000216667 mm^3; δ_{20} = -0.007519167 Nmm^2; δ_{22} = 0.24 mm; $\delta_{23} = \delta_{32}$ = -0.00475 mm^2; $\delta_{34} = \delta_{43}$ = -0.00475 mm^2; δ_{40} = 6.03167E-07 Nmm^2; δ_{44} = 0.19 mm.

To solve this system of equations, the substitution method or the elimination method is used. For this purpose, the equations are represented in matrix form as Ax = b, where A is the coefficient matrix, x is the vector of unknowns (x_1, x_2, x_3, x_4), and b is the vector of constants.

$$\begin{bmatrix}\delta_{11} & \delta_{12} & \delta_{13} & \delta_{14}\\ \delta_{21} & \delta_{22} & \delta_{23} & \delta_{24}\\ \delta_{31} & \delta_{32} & \delta_{33} & \delta_{34}\\ \delta_{41} & \delta_{42} & \delta_{43} & \delta_{44}\end{bmatrix} \cdot \begin{bmatrix}x_1\\ x_2\\ x_3\\ x_4\end{bmatrix} = \begin{bmatrix}\delta_{10}\\ \delta_{20}\\ \delta_{30}\\ \delta_{40}\end{bmatrix} \quad (21)$$

After performing the calculations, the following values are obtained: x_1 = 0.645827127 N; x_2 = 56.40412106 N · mm; x_3 = -6.155839315 N; x_4 = -229.2344189 N · mm.

Resulting diagrams:

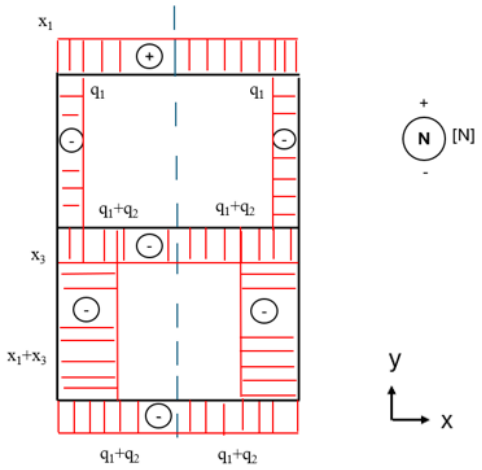

Figure 10: *Axial force diagram.*

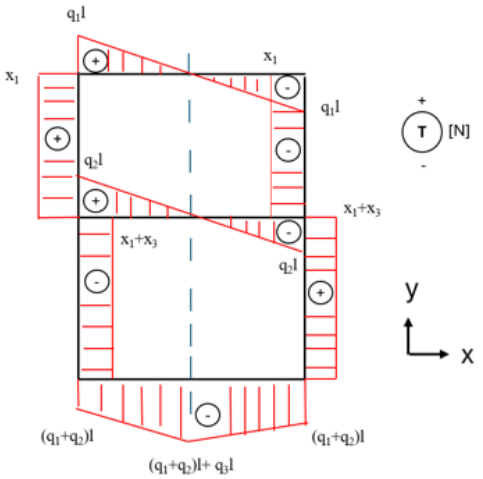

Figure 11: *Shear force diagram.*

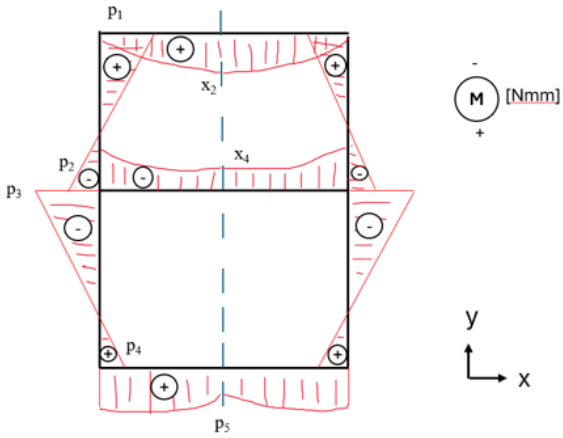

Figure 12: *Bending moment diagram*

Where:

$$P_1 = x_2 - q_1 \cdot \frac{l^2}{2} \quad (22)$$

$$P_2 = x_2 - x_1 \cdot h - q\frac{l^2}{2} \quad (23)$$

$$P_3 = x_2 - x_1 \cdot h - q_1\frac{l^2}{2} + x_4 - q_2\frac{l^2}{2} \quad (24)$$

$$P_4 = x_2 - x_1 \cdot 2h - q_1\frac{l^2}{2} + x_4 - x_3 \cdot h - q_2\frac{l^2}{2} \quad (25)$$

$$P_5 = x_2 - x_1 \cdot 2h - q_1\frac{l^2}{2} + x_4 - x_3 \cdot h - q_2\frac{l^2}{2} - q_3\frac{l^2}{2} \quad (26)$$

As a result of the calculations, the following values are obtained: P_1 = 28.05412 Nmm^2; P_2 = 4.237 mm; P_3 = 247.122 Nmm^2; P_4 = 28.378 Nmm^2; P_5 = 19.804 mm.

Based on the analysis of the moment diagram in Figure 12, it is observed that the clamped section of level 2 of the robot is the most prone to failure. Therefore, the stress is calculated at that point.

$$\sigma = \frac{M_{max}}{W_y} \quad (27)$$

Where:

1. σ represents the normal stress,
2. M_{max} represents the maximum moment resulting from the moment diagram,
3. W_y represents the section modulus.

$$W_y = \frac{I_y}{Z_{max}} \quad (28)$$

Where:

1. I_y is the moment of inertia relative to the Y-axis,
2. $Z_{max}$is the maximum distance from the neutral axis to the centroid.

To ensure calculation accuracy, the SolidWorks simulation program can be used by modeling the section of interest.

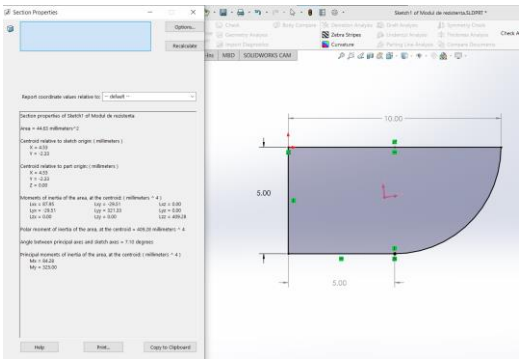

Figure 13: *Housing section with M_{max}.*

From the geometric design of the housing section experiencing the maximum moment and based on the calculations performed using the SolidWorks simulation program, it results that M_y=I_y (moment of inertia) is 84.28 mm^4.

Additionally, Z_{max} was determined by subtracting the Y-axis centroid coordinate from the total side length of 5 mm of the section. After performing the calculations, Z_{max} = 2.67 mm, which is greater than the centroid coordinate on the Y-axis of 2.33 mm.

Thus, it follows that W_y = 31.566 mm^3, and by substituting into equation 21, σ = 7.828 N/mm^2. For the PLA material from which the housing is made, $\sigma_{yield} \approx 25\ MP_a$.

In conclusion, the strength calculations indicate that the system is safe because the condition $\sigma < \sigma_{yield}$ is met.

The results demonstrate that the stack-based configuration of the mobile inverted pendulum robot effectively balances compactness, stability, and adaptability. The structure meets mechanical strength and stability requirements while offering significant advantages in scalability and ease of integration for modular enhancements.

4. Future improvements

To improve the mechanical performance of the stack-based design, several advanced strategies can be implemented:

1. material optimization: replacing PLA with high-performance materials such as carbon fiber-reinforced polymers or aerospace-grade aluminum alloys can significantly enhance strength-to-weight ratio. These materials offer

superior mechanical properties, reducing deformation under load while maintaining lightweight characteristics essential for stability.
2. dynamic load analysis: conducting detailed finite element analysis (FEA) to identify stress concentrations and deformation zones can lead to targeted structural improvements. Optimizing the distribution and geometry of load-bearing elements, such as support bars and plates, can reduce the risk of mechanical failure during operation.
3. center of gravity refinement: lowering the center of gravity further through strategic placement of heavy components like motors and batteries at the base of the stack can improve stability. A modular adjustment system could enable fine-tuning of component positions to adapt to different configurations or payloads.
4. structural reinforcements: integrating ribbed supports or honeycomb structures into the design can enhance stiffness and distribute mechanical stresses more evenly. These features also minimize material usage, achieving a balance between strength and weight.
5. vibration damping: incorporating dampening mechanisms or materials at connection points between layers can reduce the impact of dynamic vibrations, which are common during movement. This would increase operational precision and reduce wear on components over time.

By addressing these mechanical improvements, the stack-based design can evolve to meet higher standards of reliability, stability, and adaptability in diverse operating conditions.

5. Conclusion

This study highlights the effectiveness of a stack-based configuration in addressing the mechanical challenges of mobile inverted pendulum robots. By aligning mass distribution along the vertical axis, the design optimizes the robot's stability, reduces inertia, and ensures uniform load distribution. The analysis demonstrates the ability of the stack structure to withstand operational stresses while maintaining a compact and modular form factor, essential for further integration and scalability.

The research underscores the potential of the stack-based approach to serve as a reliable foundation for self-balancing systems. It not only satisfies critical requirements for mechanical stability but also supports adaptability for future enhancements. The insights derived from structural resistance calculations, material analysis, and center of gravity optimization provide a pathway for advancing the design of mobile robots, combining functionality with robust performance in diverse applications.

Acknowledgments

This work is supported by Romanian Ministry of Education, through the Agency for Loans and Scholarships.

References

1. Segway Inc., About Segway: Segway Company Milestones, 2011. [Online]. Available from: http://www.segway.com/about-segway/segway-milestones (accessed 13 December 2023).
2. Arleo, A., Millan, J. D. R., Floreano, D. Efficient Learning of Variable-Resolution Cognitive Maps for Autonomous Indoor Navigation. IEEE Trans. Robot. Autom., 1999.
3. Bekte, M., Gurvits, L. Mobile Robot Localization Using Landmark. IEEE Trans. Robot. Autom., 1997.
4. Raj, R., Kos, A. A Comprehensive Study of Mobile Robot: History, Developments, Applications, and Future Research Perspectives. July 2022. Available from: https://www.researchgate.net/deref/https%3A%2F%2Fdoi.org%2F10.3390%2Fapp12146951 (accessed 28 November 2023).
5. Everett, H. R. Sensors for Mobile Robots. 15 July 1995. Chapter 1: p. 3. https://doi.org/10.1201/9781439863480 (accessed 28 November 2023).
6. Borenstein, J. Real-time Obstacle Avoidance for Fast Mobile Robots. IEEE Trans. Syst. Man Cybern., 1989.
7. Asafa, T. B. et al. (2018) *Development of a*

vacuum cleaner robot, Alexandria Engineering Journal, 57(4), pp. 2911–2920. https://doi.org/10.1016/j.aej.2018.07.005.Jkjhk

8. Siregar, B., Hutagaol, B. M. and Salim Sitompul, O. (2020) *Smartphone-controllable lawn mower robot*, 2020 International Conference on ICT for Smart Society (ICISS) [Preprint]. https://doi.org/10.1109/iciss50791.2020.9307574Jyjyjk
9. Yuan Fu-cai et al. (2011) *Design of cleaning robot for swimming pools*, MSIE 2011 [Preprint]. https://doi.org/10.1109/msie.2011.5707629Kukuk
10. Tian, Z. and Shi, W. (2022) *Design and implement an enhanced simulator for Autonomous Delivery Robot*, 2022 Fifth International Conference on Connected and Autonomous Driving (MetroCAD) [Preprint]. https://doi.org/10.1109/metrocad56305.2022.00009Jmhmu
11. Klemm, V. et al. (2019) 'Ascento: A two-wheeled jumping robot', 2019 International Conference on Robotics and Automation (ICRA) [Preprint]. https://doi.org/10.1109/icra.2019.8793792
12. Ahmed, A. A. and Saleh Alshandoli, A. F. (2020) *On replacing a PID controller with Neural Network Controller for Segway*, 2020 International Conference on Electrical Engineering (ICEE) [Preprint]. https://doi.org/10.1109/icee49691.2020.9249811
13. Vahid Alizadeh, H. and Mahjoob, M. J. (2011) *Quadratic damping model for a spherical mobile robot moving on the free surface of the water*, 2011 IEEE International Symposium on Robotic and Sensors Environments (ROSE) [Preprint]. https://doi.org/10.1109/rose.2011.6058541
14. Mukherjee, R., Minor, M. A. and Pukrushpan, J. T. (no date) *Simple Motion Planning Strategies for SPHEROBOT: A Spherical Mobile Robot*, Proceedings of the 38th IEEE Conference on Decision and Control (Cat. No.99CH36304) [Preprint]. https://doi.org/10.1109/cdc.1999.831235
15. S. L. Podvalny and E. M. Vasiljev, Modeling of Human-Robot Physical Interaction for Case of Mobile Self-Balanced Robot, 2019 International Conference on Industrial Engineering, Applications and Manufacturing (ICIEAM), Sochi, Russia, 2019, pp. 1-5, https://doi.org/10.1109/ICIEAM.2019.8742942

.